CrossMark

Extended Pharmacokinetic Model of the Rabbit Eye for Intravitreal and Intracameral Injections of Macromolecules: Quantitative Analysis of Anterior and Posterior Elimination Pathways

Marko Lamminsalo [1] (iD) • Ella Taskinen [1] • Timo Karvinen [2] • Astrid Subrizi [3] • Lasse Murtomäki [4] •
Arto Urtti [1,5,6] • Veli-Pekka Ranta [1]

ABSTRACT

Purpose To extend the physiological features of the anatomically accurate model of the rabbit eye for intravitreal (IVT) and intracameral (IC) injections of macromolecules.

Methods The computational fluid dynamic model of the rabbit eye by Missel (2012) was extended by enhancing the mixing in the anterior chamber with thermal gradient, heat transfer and gravity, and studying its effect on IC injections of hyaluronic acids. In IVT injections of FITC-dextrans (MW 10–157 kDa) the diffusion though retina was defined based on published *in vitro* data. Systematic changes in retinal permeability and convective transport were made, and the percentages of anterior and posterior elimination pathways were quantified. Simulations were compared with published *in vivo* data.

Results With the enhanced mixing the elimination half-lives of hyaluronic acids after IC injection were 62–100 min that are similar to *in vivo* data and close to the theoretical value for the well-stirred anterior chamber (57 min). In IVT injections of FITC-dextrans a good match between simulations and *in vivo* data was obtained when the percentage of anterior elimination pathway was over 80%.

Conclusions The simulations with the extended model closely resemble *in vivo* pharmacokinetics, and the model is a valuable tool for data interpretation and predictions.

ABBREVIATIONS

2D/3D	Two/three-dimensional
AH	Aqueous humor
AMD	Age-related macular degeneration
A_{TM}	Amount of macromolecule eliminated through trabecular meshwork with aqueous drainage
AUC_a	Area under the concentration curve in the aqueous humor
C_a	Mean concentration of macromolecule in the aqueous humor (anterior chamber)
CFD	Computational fluid dynamics
C_v	Mean concentration of macromolecule in the vitreous
D	Diffusion coefficient of macromolecule in water
D_{ret}	Apparent diffusion coefficient of macromolecule in retina
f	Aqueous humor flow rate
FEM	Finite element modeling
IC	Intracameral
IOP	Intraocular pressure
IVT	Intravitreal
k_{ac}	Elimination rate constant of macromolecule from the anterior chamber

✉ Marko Lamminsalo
marko.lamminsalo@uef.fi

1 School of Pharmacy, University of Eastern Finland P.O. Box 1627 FI-70210 Kuopio, Finland

2 Comsol Oy Helsinki, Finland

3 Interdisciplinary Nanoscience Center (iNANO), Aarhus University Aarhus, Denmark

4 Department of Chemistry and Materials Science, Aalto University Espoo, Finland

5 Faculty of Pharmacy, Drug Research Program, University of Helsinki Helsinki, Finland

6 St Petersburg State University Petergoff St. Petersburg, Russian Federation

k_v	Elimination rate constant of macromolecule from the vitreous
MRI	Magnetic resonance imaging
MW	Molecular weight
P_{app}	Apparent permeability coefficient of macromolecule in membrane
PK	Pharmacokinetics
r_H	Hydrodynamic radius
RPE	Retinal pigment epithelium
$t_{1/2}$	Elimination half-life
TM	Trabecular meshwork
V_a	Volume of the anterior chamber
V_v	Volume of the vitreous

INTRODUCTION

Effective and economical drug therapies are needed for age-related macular degeneration (AMD) and other retinal diseases in the aging populations (1). Intravitreal (IVT) injections of anti-VEGF proteins are widely used in the clinics to treat the wet form of AMD (2), but there is a need for longer acting and more economical drugs and dosage forms for retinal diseases. For this reason, much emphasis is currently placed on the pharmacokinetic (PK) modeling of retinal drug delivery, especially of protein drugs (3,4).

An important feature in the posterior eye PK is that the concentration of intravitreally injected drug is not uniform in the vitreal cavity. Significant time-dependent concentration gradients of small molecules and macromolecules have been revealed in rabbit vitreous using *in vivo* fluorophotometry and magnetic resonance imaging (MRI) (5–8). The local drug concentrations in different parts of the retina and choroid dictate the efficacy and safety of the drug treatment, but they cannot be modeled with traditional compartmental modeling that assumes an even drug concentration throughout the vitreous. Instead, computational fluid dynamics (CFD) based on finite element modeling (FEM) or finite volume method (FVM) must be used, because the methods employ anatomically relevant three-dimensional (3D) geometric models that consist of thousands of tiny compartments (9–11). This allows simulation of localized drug concentrations in the posterior segment of the eye.

Since 1990's several CFD models of posterior eye segment have been developed to understand and predict the drug concentration profiles in the vitreous. These models have been used to understand roles and functions of the position and volume of IVT injection (9,10,12), different types of controlled-release formulations (8,13,14) and transscleral drug delivery (15,16). Physiological aspects like aphakia (17), vitreous substitutes (18), and vitreous liquefaction and saccadic motion (19) have also been simulated.

More recently, CFD models have been built for the complete eye enabling simultaneous evaluation of drug kinetics in the anterior and posterior segments of the eye after IVT and topical application (11,20–25). The most comprehensive study on IVT administration was published by Missel (11) who built anatomically accurate models for human, rabbit and monkey eyes based on MRI, and validated the rabbit model using published *in vivo* data on six compounds with a wide range of molecular weights (0.3–157 kDa).

The general aim of our study was to extend the rabbit model developed by Missel (11). The first specific objective was to enhance the drug elimination from the anterior chamber by producing a circulatory flow pattern of aqueous humor (AH) in this chamber. This flow pattern results from temperature and density gradients and gravity (26). Earlier, this phenomenon has been included in computational models of the anterior chamber to explain the asymmetric dilatation of the pupil after topical application of mydriatics (26,27) and the formation of hyphemas and Krukenberg spindles in a diseased or traumatized eye (28,29). In our study, the circulatory flow pattern was added into a complete ocular CFD model to describe realistically the elimination of macromolecules from the anterior chamber after intracameral (IC) and IVT injection.

The second specific objective was to use the extended model for a quantitative analysis of anterior (drainage through trabecular meshwork, TM) and posterior (permeation through retina) elimination of macromolecules after IVT injection by comparing simulated vitreal and aqueous concentrations with published *in vivo* data (30,31). Earlier, CFD models have been used to evaluate the percentages of the elimination routes theoretically without direct comparisons with *in vivo* data (14,24,25). In our model the diffusion rate through retina was defined based on our previously published *in vitro* permeability data (32). Additionally, in analogy with several previous CFD studies (11,20,24,25) the convective transport of macromolecules in the vitreous was changed systematically because a small portion of AH flows into posterior direction and this flow probably varies in different physiological conditions (6,33).

METHODS

A general description of the methods is given in this section. A more detailed description of CFD modeling is given in the Electronic Supplementary Material.

Software

The geometry of the rabbit eye was constructed using AutoCAD 2015 (Autodesk, Inc., San Rafael, CA, USA). CFD modeling based on FEM was made with Comsol Multiphysics 5.3 software (COMSOL AB,

Stockholm, Sweden). The modules for laminar flow, heat transfer in fluids, non-isothermal flow multiphysics, and transport of diluted species were used. Simulations were run with Intel Core i7–6700 16 GB RAM PC running under Windows 10.
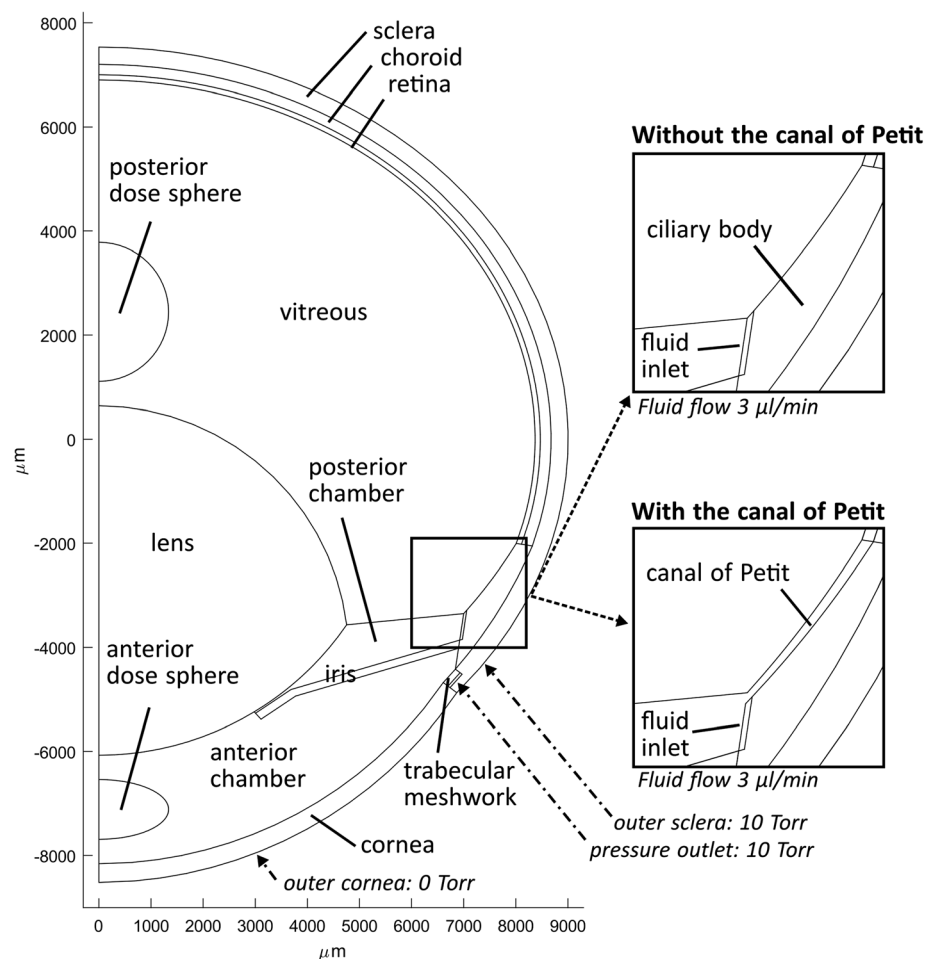
Geometry and Meshing

The rabbit's eye was based on the 2D-axisymmetric geometry by Missel (11) (Fig. 1). A symmetric 3D eye was obtained by rotating the geometry around the anterior-to-posterior axis. In the base model the minimum distance between the lens and the iris was 30 μm which enabled practically equal intraocular pressure (IOP) in the anterior and posterior chambers (no valve-effect). The geometry without the canal of Petit was used in the simulations unless otherwise stated. The thickness of the canal of Petit was 100 μm. The geometry was divided into 36,613 mesh elements.

Materials

The properties of rabbit ocular tissues are presented in Table I. TM was assumed to have the same thermal conductivity and specific heat as cornea.

Formation and Outflow of Aqueous Humor

The flow of AH was defined based on Missel (11) using incompressible flow of water with Navier-Stokes equations in free flow and Brinkman equations in porous media. The dynamic viscosity of water was 7.32–6.89×10^{-4} kg m^{-1} s^{-1} at 34–37°C in all tissues. AH was formed in the inlet port of the posterior chamber (Fig. 1) at the rate of 3 μl min^{-1}. In our model, this inflow was defined as the influx velocity of 0.1332 mm min^{-1} (without Petit's canal) or 0.1655 mm min^{-1} (with Petit's canal) which were obtained by dividing 3 mm^3 min^{-1} by the surface area of the inlet port. The flow pattern of AH in the eye was governed by the porosity and hydraulic permeability of the tissues (Table I), and by the pressures (Fig. 1). Lens, iris and ciliary body were set impermeable to fluid. Fluid flow from the posterior chamber back to the inlet port and from the fluid outlet ports (outer cornea, posterior choroid and TM) back to the inner eye was not allowed. The pressure in the outlet port behind TM and at outer sclera was set to 10 Torr, and that at outer cornea to 0 Torr, respectively. The hydraulic permeability of TM was adjusted to produce the desired IOP values of 10.1, 12.5, 15, 17.5 and 20 Torr, respectively. For each pair of IOP and

Fig. 1 2D-axisymmetric geometry of rabbit's eye based on Missel (11). The area around the fluid inlet is shown in inserts without and with the canal of Petit. The external pressures at outer cornea, outer sclera and pressure outlet are also shown.

Table I Properties of the Rabbit Ocular Tissues

Tissue	Thermal conductivity (W m^{-1} K^{-1})	Specific heat[a] (J kg^{-1} K^{-1})	Density[b] (kg m^{-3})	Porosity[c]	Hydraulic permeability[c] (m^2)
Cornea	0.52[a]	3600	1050	1	1.04×10^{-18}
Aqueous humor	0.62[d]	4177[d]	994–995[d]	0	–
Iris/ciliary body	0.52[a]	3600	1100	–[f]	–[f]
Lens	0.40[e]	3000	1050	–[f]	–[f]
Vitreous	0.60[e]	3900	1000	1	5.8×10^{-14}
Retina/ Choroid/ Sclera	0.52[a]	3600	1100	1	1.04×10^{-18}
Trabecular meshwork	0.52[a]	3600	1050	1	Adjusted[g]

– not applicable; [a] Ref (34); [b] Ref (35); [c] Ref (11), hydraulic permeability obtained as the inverse of hydraulic resistivity; [d] Built-in value in Comsol Multiphysics for water at 34–37°C; [e] Ref (36); [f] Impermeable to fluid; [g] Described in Formation and outflow of aqueous humor.

hydraulic permeability of TM (given in Results), the steady-state fluid flow pattern and pressure contour were simulated, and the fluid outflow (μl min^{-1}) through TM, retina, and cornea was determined. The increase in IOP directed more fluid toward the posterior eye and through retina, and at 20 Torr the simulated fluid outflow through retina was the same as the mathematically estimated fluid outflow in *in vivo* rabbit study by Araie and Maurice (6) (see Results). This was a technical way to study the effects of convection on drug distribution and elimination, and not a physiological description of water transport across retina because osmotic and oncotic gradients across retina, and hydrostatic pressures in choroidal tissue, choriocapillaris and suprachoroid were not considered (33,37). In addition, the fluid outflow through TM was considered to include the uveoscleral outflow.

Enhanced Mixing in the Anterior Chamber with Heat Transfer

A circulatory motion of AH in the anterior chamber was generated with temperature gradient, heat transfer, and gravity based on the model by Karampatzakis and Samaras (38). The temperature of sclera, choroid, retina and aqueous humor inlet was set to 37°C, and that of cornea to 34°C (29,39,40). Heat transfer from the posterior eye towards the cornea was defined using a convection-diffusion equation for heat conservation based on thermal conductivity and specific heat of the tissues (Table I) which created a temperature gradient in the eye. Gravity was set along the symmetry axis from anterior to posterior eye. This orientation (a horizontal head with eyes looking up) is not physiologically relevant for the rabbit, but the only option in 2D-axisymmetric model. Later, the model with the combination of temperature gradient, heat transfer and gravity is called simply as the model with heat transfer.

Transport of Macromolecules by Convection and Diffusion

The transport of the macromolecules were defined with a convection-diffusion equation for conservation of species. The flow pattern of AH described above carried macromolecules by convection. Diffusion of macromolecules in the anterior and posterior chambers was defined using diffusion coefficients (D) in water (see below). Diffusion of FITC-dextrans in the vitreous was also based on D in water using same assumption as Missel (11). Diffusion of FITC-dextrans through retina was defined using apparent retinal diffusion coefficients (see below), and the sink with zero concentration was at the anterior surface of the choroid. Diffusion coefficient of macromolecules in TM was the same as in AH, but convection was the dominant transport mechanism in TM. All the other boundaries in the eye were impermeable to macromolecules. Thus, the only elimination routes of macromolecules were through TM (anterior pathway) and retina (posterior pathway).

Diffusion Coefficients of Macromolecules in Water and in Retina

Diffusion coefficients of FITC-dextrans in water (37°C) were taken from Missel (11) (Table II). Diffusion coefficients of hyaluronic acids (D; cm^2 s^{-1}) were calculated at 20°C from their molecular weight (MW; Da) using Eq. 1 based on published data (41) and then scaled to 37°C using Eq. 2:

$$D_{20} = 0.00001408 \times MW^{-0.58217} \tag{1}$$

$$D_{37} = \frac{T_{37}\eta_{20}}{T_{20}\eta_{37}} \times D_{20} \tag{2}$$

where T is absolute temperature and η viscosity of water. Apparent diffusion coefficients of FITC-dextrans in retina

Table II Diffusion Coefficients of Macromolecules in Water (D) and in Retina (D_{ret}) at 37°C

Molecule	MW (kDa)	D ($\times 10^{-6}$ cm^2 s^{-1})	r_H (nm)	P_{app} ($\times 10^{-7}$ cm s^{-1})	D_{ret} ($\times 10^{-9}$ cm^2 s^{-1})
FITC-dextran D10	10.5	1.62	2.03	2.01	2.01
FITC-dextrans D66 and D67[a]	66–67	0.606	5.42	0.393	0.393
FITC-dextran D157	157	0.386	8.51	0.0887	0.0887
Hyaluronic acid HA18	18	0.727	–	–	–
Hyaluronic acid HA500	500	0.105	–	–	–
Hyaluronic acid HA4000	4000	0.0313	–	–	–

MW molecular weight, r_H hydrodynamic radius, P_{app} apparent permeability coefficient in bovine retinal pigment epithelium-choroid preparation *in vitro*, − not applicable

[a] D66 and D67 were considered identical molecules in simulations whereas separate *in vivo* data were available

(D_{ret}) were estimated from *in vitro* permeability data in bovine retinal pigment epithelium (RPE)-choroid preparations (32) assuming that RPE is the rate-limiting barrier in retina and the retinal barrier in rabbit is similar to bovine based on the similar basic structure of RPE in these species (e.g., tight junctions) (42,43). The apparent permeability coefficients (P_{app}; cm s^{-1}) of FITC-dextrans (4–80 kDa) (32) *versus* hydrodynamic radius (r_H; nm) were described with Eq. 3 using r_H *vs.* MW relationship from published data (44):

$$P_{app} = \exp(-14.4428) \times \exp(-0.4816 \times r_H) \quad (3)$$

This equation was used to estimate P_{app} for FITC-dextrans shown in Table II. These were converted to D_{ret} using the definition of P_{app} (Eq. 4):

$$P_{app} = \frac{D_{ret} \times K}{h} \quad (4)$$

where K is the partition coefficient between retina and water and h the thickness of the retina (100 µm in this model). For technical convenience, K was assumed to be 1 and D_{ret} was obtained with Eq. 5:

$$D_{ret} = P_{app} \times h \quad (5)$$

Simulations of Intracameral and Intravitreal Injections

IC dose of hyaluronic acids was defined as an even initial concentration (1 mM) either in the whole anterior chamber (248 µl) or in the anterior dose sphere (4.3 µl), respectively (Fig. 1). IVT dose of FITC-dextrans was given in the posterior dose sphere (10 µl). Simulations were made with and without the heat transfer, and the simulations of IVT injections also with and without the canal of Petit were conducted. Additionally, the simulations of IVT injections were made with three different settings for the retinal permeability of FITC-dextrans: 1) impermeable retina (only fluid passed retina), 2) diffusion though retina was allowed, but convection

through retina was blocked meaning that convection was allowed to carry molecules only to the anterior surface of retina, whereas the transport of FITC-dextrans through retina was purely diffusive (fluid passed retina, but fluid flow velocity for convective transport in retina was set to zero), 3) convection of FITC-dextrans though retina was allowed in such a way that the retina did not offer any hindrance for convective transport. The simulation was carried out in two steps. First, the steady-state flow pattern of the AH in the eye was calculated. Second, the time-dependent concentration profile of macromolecule was simulated. Solutions were calculated with the default solver using backward differentiation formula and the largest possible integration steps. This was achieved by means of an adaptive step size. The step was accepted if it fulfilled the requirement for the error estimate, otherwise it was adapted. The length of the simulations for IC and IVT injections were 600 min and 3000 h, respectively. The simulation of IVT injection typically lasted 1 min.

Pharmacokinetic Parameters and Model Validation

For IC injections of hyaluronic acids, one or two elimination rate constants from the anterior chamber (k_{ac}) and the corresponding elimination half-lives ($t_{1/2}$) were determined based on the shape of log(concentration) *vs.* time curve using Phoenix WinNonlin version 6.3 software (Certara, Princeton, NJ, USA). The simulations were compared with the corresponding *in vivo* data (45) and with the theoretical half-life in a well-stirred anterior chamber:

$$t_{1/2} = \frac{ln2 \times V_a}{f} = \frac{ln2 \times 248\,\mu l}{3\,\mu l\ min^{-1}} = 57 min \quad (6)$$

where V_a is the volume of anterior chamber, and f is the AH flow rate. For IVT injection of FITC-dextrans, the elimination rate constant from the vitreous (k_v) and the corresponding elimination half-life ($t_{1/2}$) were determined from the log-linear portion of the vitreous concentration *vs.* time curve. The ratio of mean aqueous (anterior chamber) to mean vitreous

concentration (C_a/C_v) was determined at 200 h where this ratio had already stabilized. These values were presented in a log-log plot of (C_a/C_v) *vs.* k_v based on the theoretical Eq. 7 by Maurice (46,47) that is valid for those compounds that are eliminated from the vitreous only via the anterior pathway with the aqueous drainage:

$$\frac{C_a}{C_v} = \frac{V_v}{f} k_v \tag{7}$$

where the theoretical slope is the ratio of vitreous volume (V_v; 1.52 ml) to f (3 µl min^{-1}), and this slope was marked in the plot. The corresponding *in vivo* data of D10, D66, D67 and D157 (30,31) were added in the same plot that is called later as Maurice plot.

The cumulative amount of FITC-dextran eliminated through the anterior (outlet port behind TM) and posterior (posterior retina) pathways was integrated with Comsol Multiphysics and is presented as the percentage of dose. The cumulative amount of macromolecule eliminated through TM (A_{TM}) was also determined using the theoretical Eq. 8:

$$A_{TM} = f \times AUC_a \tag{8}$$

where AUC_a in the area under the aqueous concentration curve (anterior chamber).

RESULTS

Aqueous Humor Flow Distribution in the Eye

The outflows though TM, retina and cornea were changed by adjusting the hydraulic permeability of TM to get the desired IOP values (Table III). The increase of IOP from 10.1 to 20 Torr lead to a 100-fold and 2-fold increases in the outflows through retina and cornea, respectively, while TM remained the major route with a minor decrease in the outflow. The outflow through retina at 20 Torr (0.1 µl min^{-1}) was the same as the experimental value by Araie and Maurice (6). The fluid velocity and pressure contours in the eye at 15 Torr are shown in Electronic Supplementary Material (Figs. S2 and S3).

Without heat transfer the outflows through TM, retina and cornea differed less than 1%, 2 and 6% from those with heat transfer, respectively.

Aqueous Humor Flow Pattern in the Anterior Chamber

The temperature difference between the anterior and posterior eye and heat transfer created a temperature gradient (Fig. 2). Without heat transfer the center of anterior chamber was poorly mixed and the maximum fluid velocity in the anterior chamber (excluding the region close to iris tip) was approximately 0.002 mm s^{-1} (Fig. 3a). The combination of heat transfer and gravity markedly increased the fluid velocity in the anterior chamber and produced a circulatory flow (Fig. 3b). The direction of gravity was from the anterior to posterior eye. Because AH entering the anterior chamber was warmer (approx. 37°C) and less dense than elsewhere in the anterior chamber it was elevated towards the cornea, being slightly cooled close to cornea and turned towards the anterior chamber angle. At the chamber angle part of AH escaped through TM, while the rest of the fluid started a new cycle. The maximum velocity of the whirl was approximately 0.02 mm s^{-1}. The flow patterns were similar between 10.1 and 20 Torr.

Intracameral Injection of Hyaluronic Acids

IC injection was initially simulated with a uniform initial concentration in the whole anterior chamber. Without heat transfer, hyaluronic acids were eliminated fairly rapidly from the peripheral anterior chamber whereas the elimination from the central region was poor (Fig. 4a-c). For this reason, two distinct phases appeared in the aqueous concentration curves and the simulated half-life of the latter phase was much higher than in *in vivo* study (Fig. 5 and Table IV). The enhanced mixing obtained with heat transfer augmented the elimination of hyaluronic acids from the whole anterior chamber (Fig. 4d-f). For HA500 and HA4000, two phases appeared in the concentration curve, but the initial fast phase ended soon (Fig. 5). With heat transfer, the simulated elimination half-life of HA18 and those of the second phase for HA500 and

Table III Aqueous Humor Outflow through Trabecular Meshwork (TM), Retina and Cornea at Different Intraocular Pressures in the Model with Heat Transfer

Intraocular pressure (Torr)	TM hydraulic permeability ($\times 10^{-16}$ m^2)	Outflow (µl min^{-1})			Fluid velocity at retinal surface[a] ($\times 10^{-7}$ cm s^{-1})
		TM	Retina	Cornea	
10.1	202.5	2.917	0.001	0.060	0.034
12.5	7.797	2.878	0.025	0.075	0.84
15	3.840	2.837	0.051	0.091	1.7
17.5	2.522	2.796	0.076	0.107	2.6
20	1.863	2.755	0.102	0.123	3.4

[a] Mean value obtained by dividing the outflow through retina by the retinal surface area (4.96 cm^2)
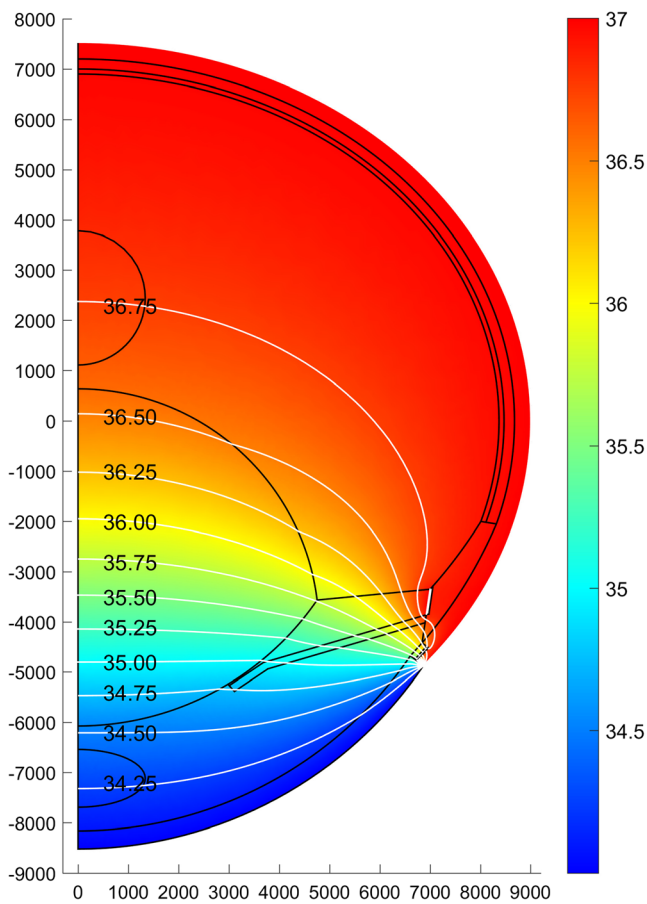
Fig. 2 Temperature gradient (°C) in the eye. The white lines represent isothermal contours.

HA4000 were similar to *in vivo* data (Table IV), and all these values were fairly close to the theoretical value for a well-stirred anterior chamber (57 min).

When the dose was placed in the anterior dose sphere the model with heat transfer produced almost similar results to those shown in Fig. 5 (a short lag time was observed), whereas without heat transfer the elimination was very slow (Figs. S4 and S5 in Electronic Supplementary Material). Further tests were conducted using the model without heat transfer. When the shortest distance between the lens and iris was reduced from 30 μm to 4 μm to get an enhanced jet of AH into the anterior chamber the performance of the model did not improve markedly (the rate constants were 95–113% of those in Table IV). Furthermore, the reduced gap acted as a pressure valve and the pressure at the posterior eye was 0.6 Torr higher than in the anterior chamber. When the diffusion coefficient (D) of HA500 in AH was set to an extremely high value (10^7 cm^2 s^{-1}) the anterior chamber behaved as a well-stirred compartment and the simulated elimination half-life of HA500 was 62 min.

Intravitreal Injection of FITC-Dextrans

General Description of Simulated Concentrations

IVT injections of FITC-dextrans were initially simulated with heat transfer and without the canal of Petit. Figure 6a shows representative concentration curves for D157. Generally, after the initial distribution phase, the vitreal concentrations (C$_v$) of FITC-dextrans declined exponentially enabling the determination of vitreal elimination rate constant (k$_v$) and the corresponding elimination half-life (t$_{1/2}$). The aqueous concentrations (C$_a$) peaked between 50 and 100 h followed by the elimination with the same rate constant as the vitreal concentrations. The aqueous to vitreous concentration ratio (C$_a$/C$_v$) was stable after 200 h. Fig. 6b shows the concentration contour at 200 h from the same simulation. In this simulation, the vitreal concentration declined in the posterior to anterior direction revealing that the diffusion towards the anterior eye dominated over the diffusion through the retina.
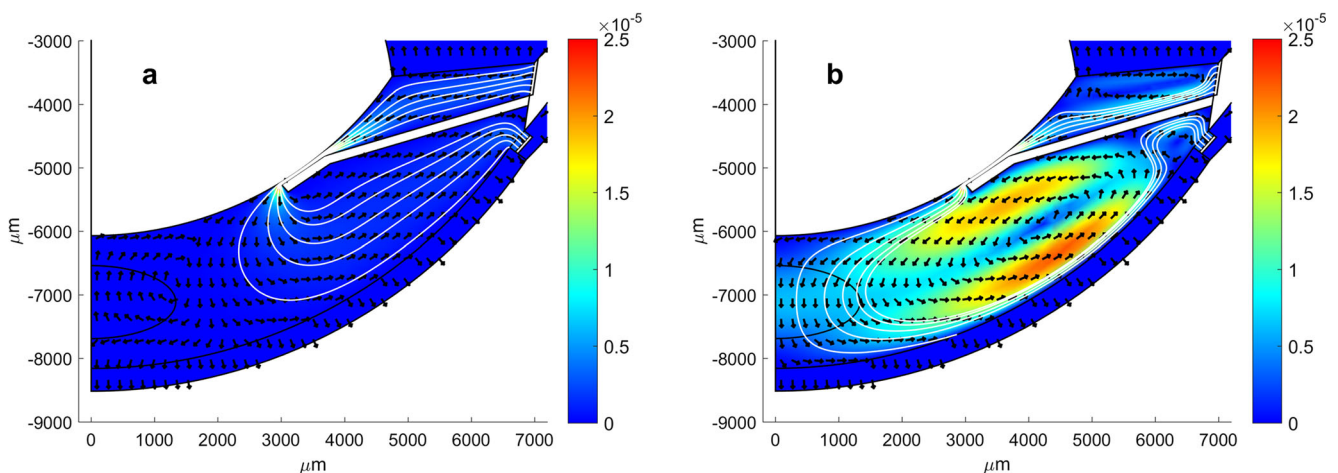
Fig. 3 Aqueous humor velocity (m s^{-1}) and flow pattern in the anterior chamber at 15 Torr without (**a**) and with (**b**) the temperature gradient, heat transfer and gravity.

Without heat transfer
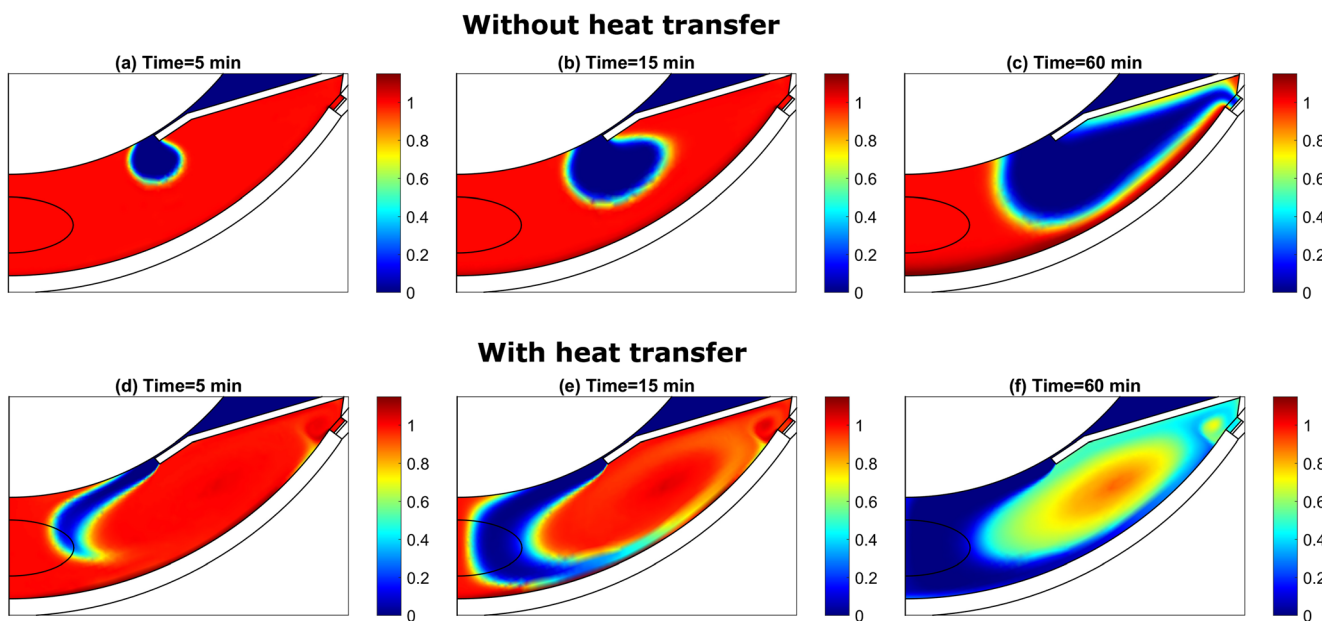
Fig. 4 Concentration gradient of HA500 in the anterior chamber at 5, 15 and 60 min after intracameral injection at 15 Torr without (upper panels) and with (lower panels) heat transfer. At time zero the concentration was uniform (red color) in the whole anterior chamber.

Impermeable Retina

When the retina was set impermeable to FITC-dextrans the simulated C_a/C_v and k_v values were close to the theoretical line in Missel plot (Fig. 7a). At 10.1 Torr k_v values of D10, D66, D67 and D157 were 118, 91, 97 and 66% of the *in vivo* values, respectively. The simulated k_v values decreased with increasing IOP. This was caused by the enhanced fluid flow rate toward posterior eye and through retina (Table III), i.e., the increased convective transport of FITC-dextrans toward the posterior vitreous reduced their diffusion toward the anterior chamber. The simulated C_a/C_v ratios also decreased with increasing IOP.

Diffusion through Retina Was Allowed

When diffusion of FITC-dextrans through retina were defined based on *in vitro* permeability experiments, k_v values increased slightly in comparison with impermeable retina (Fig. 7b). All simulated k_v values for D157 were still lower than *in vivo*. At 10.1 Torr the percentage of posterior elimination pathway for D10, D66/D67, and D157 was 20%, 11%, and 4%, respectively (Table V). The simulated data points for D10 were markedly below the theoretical line because of the increased portion eliminated via the posterior pathway. Generally, an increase in IOP resulted in an increase in the portion of posterior pathway (Table V) and a decrease in k_v (Fig. 7b). This

Fig. 5 Mean concentration of hyaluronic acids in the anterior chamber after intracameral injection at 15 Torr without (**a**) and with (**b**) heat transfer. Simulated concentrations (fraction of initial value) are shown as lines, and corresponding *in vivo* data (45) as circles. At time zero the concentration was uniform in the whole anterior chamber.
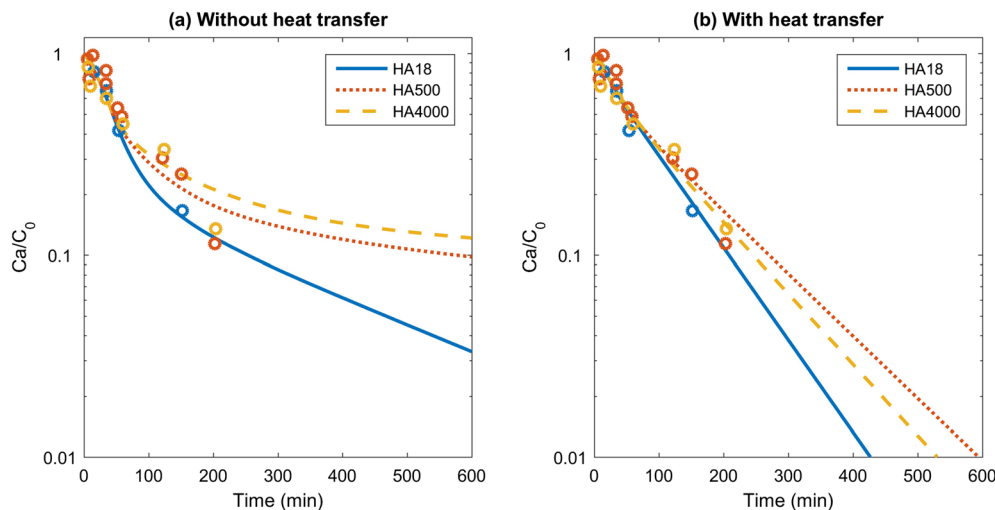
Table IV　Elimination of Hyaluronic Acids from the Anterior Chamber after Intracameral Injection with the Uniform Initial Concentration in the Whole Anterior Chamber

Molecule	Without heat transfer		With heat transfer		In vivo data[a]	
	k_{ac} ($10^{-3} \times$ min^{-1})	$t_{1/2}$ (min)	k_{ac} ($10^{-3} \times$ min^{-1})	$t_{1/2}$ (min)	k_{ac} ($10^{-3} \times$ min^{-1})	$t_{1/2}$ (min)
HA18	22.2; 2.71	31; 256	11.3	62	11.1 ± 1.1	62 (44–109)
HA500	21.5; 1.44	32; 482	28.9; 6.96	24; 100	9.7 ± 0.6	71 (63–83)
HA4000	23.3; 1.51	30; 459	28.6; 8.02	24; 86	8.4 ± 0.6	83 (69–103)

k_{ac} elimination rate constant from the anterior chamber; $t_{1/2}$ elimination half-life; two k_{ac} and $t_{1/2}$ values were estimated when there were two phases in the concentration curve. IOP was 15 Torr and the shortest distance between lens and iris 30 μm

[a] Ref (45) with k_{ac} as mean ± SD, and $t_{1/2}$ as mean (95% confidence interval)

means that concerning the total elimination rate from the vitreous (k_v) the increased elimination via the posterior pathway at higher IOP values did not fully compensate for the hindered diffusion toward the anterior eye.

Convection through Retina Was Allowed

When the fluid flow through retina was allowed carry FITC-dextrans across retina by convection without any sieving effect of retina, k_v values increased with IOP because of enhanced posterior fluid flow (Fig. 7c). For example, the fluid velocity through retina at 20 Torr was 3.4×10^{-7} cm s^{-1} (Table III) that was much higher than P_{app} values of D66/D67 and D157 (Table II). For this reason the convective transport of D66/D67 and D157 through retina at 20 Torr was much faster than the diffusion through retina in the previous simulations (Fig. 7c vs. b). At higher IOPs the simulated data points for D66/D67 and D157 deviated markedly from in vivo data, and the posterior pathway became the dominating elimination route (Table V).

### Effect of Removing Heat Transfer or Adding the Canal of Petit

When heat transfer was removed from the model with retinal diffusion, the percentage of posterior elimination pathway, k_v and C_a/C_v values of FITC-dextrans were 96–105% of those with heat transfer, respectively. The canal of Petit had a slightly larger effect. When the canal was added to the model with heat transfer and retinal diffusion, k_v values increased by 9–21% and C_a/C_v values decreased by 2–8%, respectively, but these changes did not improve the overall match between simulated and in vivo data when all other model parameters were fixed (Fig. 8; compare with Fig. 7b). At the same time the relative decrease in the percentage of posterior elimination pathway was 8–17%.

Parameter Sensitivity Analysis for D157

The model with heat transfer and retinal diffusion was considered to be the most relevant basic model (Fig. 7b). However, the simulated C_a/C_v and k_v values for D157 were

Fig. 6 Simulated concentrations of D157 after intravitreal injection: (**a**) the mean vitreal (C_v) and aqueous (C_a) concentrations (log scale on the left) and aqueous to vitreous concentration ratio (C_a/C_v) (scale on the right); (**b**) the concentration contour at 200 h. The model with heat transfer and without the canal of Petit was used at 15 Torr. Diffusion of D157 through the retina was allowed in this simulation.

(a) Log C and Ca/Cv versus time

(b) Concentration at time = 200 h
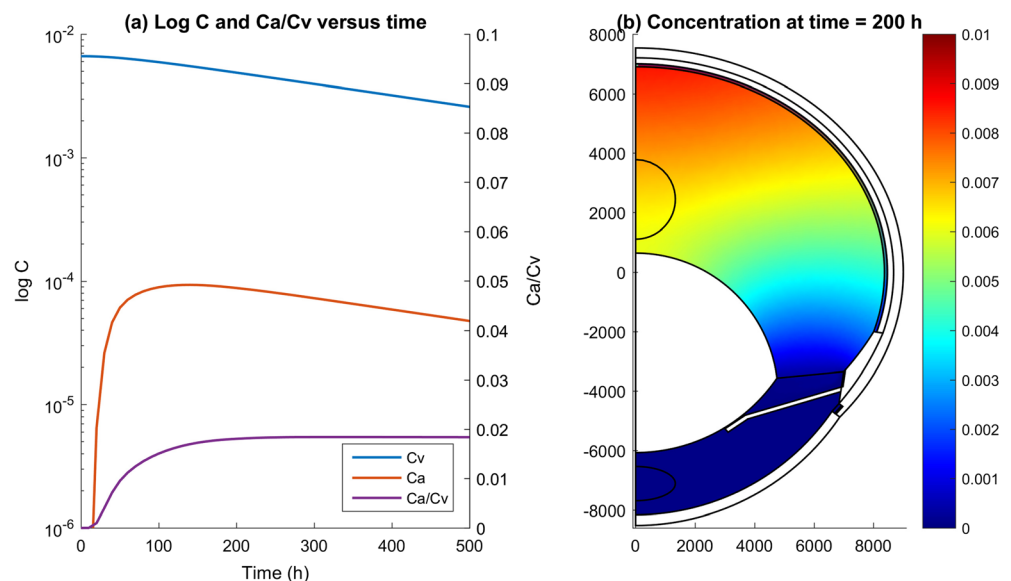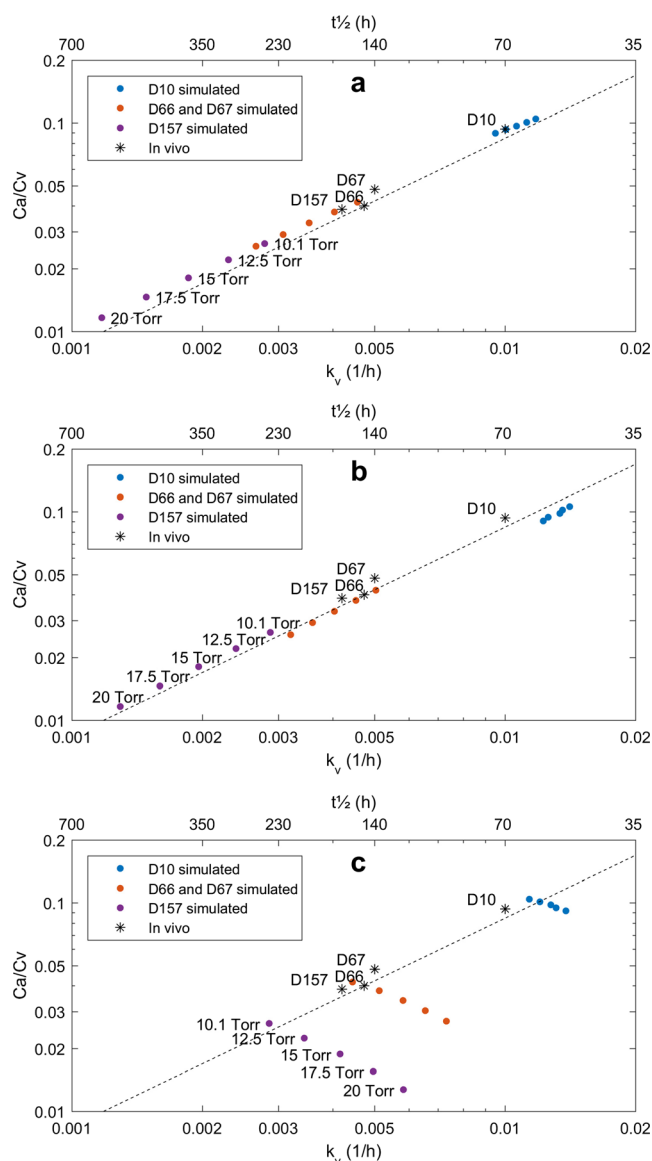
Fig. 7 Maurice plot of simulated and *in vivo* data (30,31) of FITC-dextrans after intravitreal injection. Simulations were made with impermeable retina to FITC-dextrans (**a**), with diffusion through retina (**b**), and with convection through retina (**c**). Fluid passed the retina in all options. Aqueous to vitreous concentration ratio (C_a/C_v) is shown on the vertical axis, and the elimination rate constant from vitreous (k_v) and the corresponding elimination half-life ($t_{1/2}$) on the lower and upper horizontal axes. Simulated values are shown for different intraocular pressures, and the order of values is always the same as shown for D157. A dashed line shows the theoretical line for those compounds that are eliminated only via the anterior route by aqueous drainage. The model with the heat transfer and without the canal of Petit was used.

significantly lower than *in vivo* values at all IOPs, and therefore, parameter sensitivity analysis was performed for this compound. When D_{ret} of D157 was increased 10-fold the simulated k_v at 10.1 Torr was close to *in vivo* value, but the simulated C_a/C_v was much lower than *in vivo* (Fig. 9a). This change increased the percentage of posterior pathway at 10.1 Torr from 4.1% (Table V) to 29.7%. The model performance was much more sensitive to the changes in diffusion coefficient (D)

of D157 (same value in water and vitreous). When D was increased by 50% the simulated C_a/C_v and k_v values for D157 at 10.1 Torr were similar to *in vivo* values (Fig. 9b). The percentage of posterior elimination pathway at 10.1 Torr decreased slightly from 4.1 to 2.9% (Table V).

Percentage of Anterior Elimination Pathway Using Aqueous AUC

The simulated amounts and percentages of FITC-dextrans eliminated via the anterior pathway were calculated using Eq. 8 for the model with heat transfer and retinal diffusion all IOP values. When the exact outflow through TM (Table III) was used as f in Eq. 8 the calculated percentages were 100–103% of those obtained with the integration function of Comsol software (the latter in Table V, 100% minus the value given with diffusion). This indicated that the mass balance was correct in the model. This calculation method is expected to be useful in PK data analysis of macromolecules (see Discussion).

DISCUSSION

Model Performance

The general objective of this study was to extend the CFD model of the rabbit eye developed by Missel (11). Our base model without heat transfer was identical to Missel based on similar hydraulic permeability values in TM to obtain IOP values of 10.1, 15 and 20 Torr (Table III) which resulted in similar fluid flow and pressure contours in the vitreous (Figs. S2 and S3 in Electronic Supplementary Material). After converting hydraulic permeability to hydraulic resistance in TM, our values were 86–91% of Missel's values.

In our study, the mixing in the anterior chamber was enhanced by producing a circulatory flow pattern with temperature gradient, heat transfer and gravity based on the model by Karampatzakis and Samaras (38). We used anterior-to-posterior direction of gravity to be able to work with the 2D axisymmetric model. With this model the simulated IC injections of hyaluronic acids closely matched with *in vivo* data (45), and the elimination half-lives of the compounds were close to the theoretical value for the well-stirred anterior chamber. Yablonski *et al.* (48) observed earlier that the anterior chamber of rabbits is well-mixed. We think that the enhanced mixing is essential for the CFD simulations of drug concentrations in AH after IC and topical drug administration.

We also found that the anterior chamber behaved as a well-stirred compartment without heat transfer if the diffusion coefficient of the macromolecule in this chamber was set to an extremely high value. However, in this case the CFD model does have any advantage over a traditional compartmental model. Furthermore, it needs to be remembered that the

Table V Simulated Elimination of FITC-dextrans Via the Posterior Pathway after Intravitreal Injection when Diffusion or Convection through Retina was allowed

Intraocular pressure (Torr)	Posterior elimination of D10 (% of dose)		Posterior elimination of D66 and D67 (% of dose)		Posterior elimination of D157 (% of dose)	
	With diffusion	With convection	With diffusion	With convection	With diffusion[a]	With convection
10.1	20.1	0.4	11.0	1.0	4.1/2.9	1.6
12.5	21.0	10.0	12.4	23.1	5.1/3.3	33.3
15	22.0	19.0	14.2	40.9	6.4/3.9	55.5
17.5	23.0	27.2	16.2	54.5	8.0/4.6	70.4
20	24.1	34.5	18.5	65.1	10.1/5.4	80.3

The remaining portion was eliminated via the anterior pathway. The mass balance at the end of simulation was 98–102% of the dose

[a] Value with the original diffusion coefficient (D) in water and vitreous (Fig. 7b)/value with 1.5 × D (Fig. 9b)

anterior chamber is not truly a well-stirred compartment with an instantaneous uniform concentration. Instead, the physiological circulatory flow pattern obtained with the CFD model may be crucial for realistic simulations. This has been shown with the more physiological, forward-looking eye using more complicated 3D models. In this case AH flows upward near the warmer iris and downward near the cooler cornea producing a mixing whirl. This provides an explanation for the asymmetric dilatation of the pupil after topical application of mydriatics (26,27) and for the location of hyphemas and Krukenberg spindles in the anterior chamber of a traumatized eye (28,29).

The effect of heat transfer on our simulations of IVT injection of FITC-dextrans was fairly small as the relative changes in the percentage of posterior elimination pathway, k_v and C_a/C_v values were less than 5%. This is explained by the fact that after IVT injection the diffusion of the macromolecule in the vitreous is the rate-limiting step for the elimination via the anterior route (46,49,50).
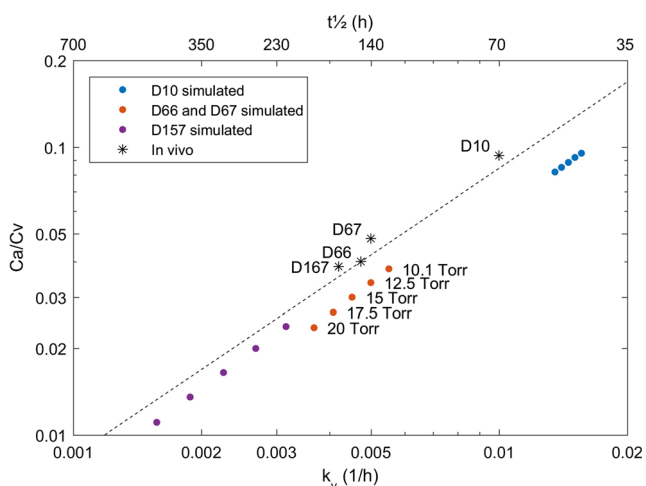
Fig. 8 Maurice plot of simulated and *in vivo* (30,31) data on FITC-dextrans after adding the canal of Petit. The model with heat transfer and retinal diffusion was used.

The extended model was used in a quantitative analysis of anterior and posterior elimination pathways of FITC-dextrans after IVT injection. In this analysis, systematic changes in retinal permeability and convective transport were made. Simulated and *in vivo* data were shown in Maurice plot (Fig. 7) where the location of the data point close to the theoretical line suggests that the anterior route is dominant (46,47). In the retinal diffusion model (Fig. 7b) the diffusion of FITC-dextrans through the retina was defined based on our previously published *in vitro* data on bovine RPE-choroid preparations (32) assuming that RPE is the rate-limiting barrier. Bovine data was used because the corresponding rabbit data are not available. With this model the simulated percentage of the posterior pathway for D10, D66/D67 and D157 at 10.1 Torr was 20%, 11% and 4%, respectively (Table V). At 10.1 Torr the simulated data point for D66/D67 was close to *in vivo* values for D66 and D67 (Fig. 7b), whereas the fit for D157 was markedly improved by increasing the original diffusion coefficient (D) in the aqueous humor and vitreous by 50% (Fig. 9b) which decreased the percentage of the posterior pathway to 3%. In the case of D10 the simulated data point with impermeable retina (Fig. 7a) was closer to *in vivo* data than that with retinal diffusion model (Fig. 7b). Overall, these simulations suggest that percentage of the posterior elimination route is below 20% for D10 and D66/67, and below 10% for D157, respectively. These estimates are similar to the published values for 50–150 kDa antibodies (13–18%) determined with a semi-mechanistic 3-compartment model (3).

As described above the best match between simulated and *in vivo* data was generally obtained at 10.1 Torr where the fluid flow through the retina (Table III) and the resulting convective transport of macromolecules in the vitreous toward the posterior eye was very low. The published estimates of the fluid flow through retina vary from practically zero (51) to 0.1 µl min⁻¹ (6) for rabbit, and up to 2.9 µl min⁻¹ for monkey with an experimental retinal detachment (33). These estimated were usually obtained with a mathematical analysis of the transport of fluorescent probes. More accurate quantitative data on the
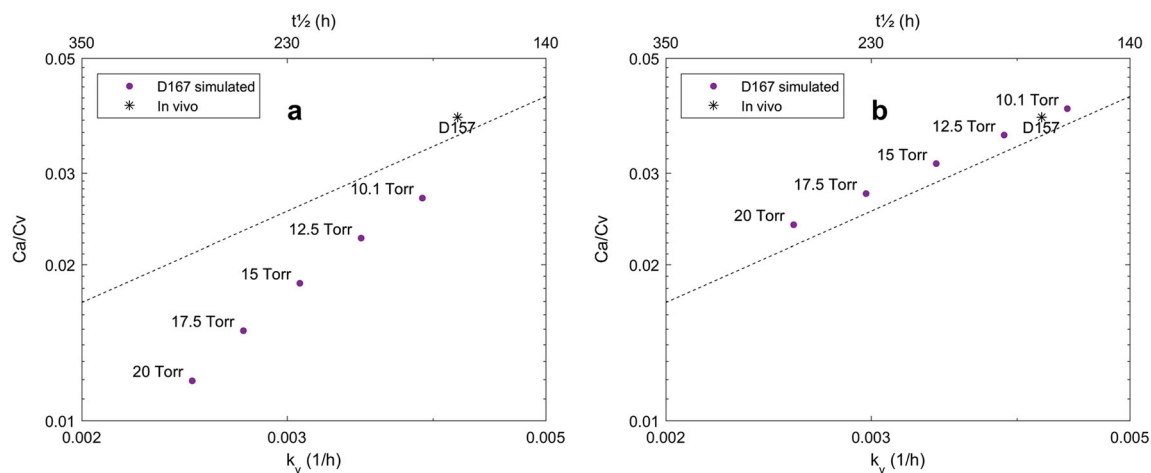
Fig. 9 Maurice plot of simulated and *in vivo* data (30) on D157 in the parameter sensitivity analysis. The apparent retinal diffusion coefficient (D_{ret}) of D157 was increased 10-fold (**a**) or the diffusion coefficient of D157 (D) in the aqueous humor and vitreous was increased by 50% (**b**). The model with heat transfer and retinal diffusion was used.

fluid flow are needed before a definite answer on the role of the convective transport can be given. Hopefully in the future, novel imaging methods will allow a direct measurement of fluid outflow through retina and other pathways in healthy and diseased eyes of laboratory animals.

Our simulations with an unrestricted convection through retina (Fig. 7c) were similar to Fig. 19 in Missel (11). However, we think that this setting is not physiologically relevant (we prefer retinal diffusion model) and it also substantially increased the percentage of the posterior pathway at higher IOP values (Table V). Additionally, we confirmed Missel's (11) finding that the canal of Petit affects the simulated concentrations to some extent (Fig. 8), but more accurate determination of *in vivo* geometry of this canal is needed before its importance can be properly estimated.

Regarding the limitations of our study, we compared simulated IVT injections of FITC-dextrans with *in vivo* data by Johnson and Maurice (30) and by Araie (31) who did not show full vitreal and aqueous concentrations curves. In the future, the performance of the extended model should be challenged by comparing simulations with the full concentration curves which will enable the parameter estimation with the curve fitting (52). The comparison with time-dependent vitreal concentrations gradients, e.g., from the posterior surface of lens to the retinal surface, is very valuable when such data are available (8,10). Furthermore, it would be important to model the drug concentrations in retina and possibly in other posterior tissues. Recently, antibody concentrations in the vitreous, retina, and aqueous were simultaneously modeled with a semi-mechanistic 3-compartment model, and separate permeability coefficients were estimated for the inner limiting membrane and RPE (3). The advantages of CFD models over compartmental models include the possibilities to model local drug concentrations (no well-stirred compartments) and to incorporate physiological mechanisms in a more realistic manner.

In summary, we have built an extended 3D model for ocular kinetics of macromolecules. The model takes into account in a realistic manner: 1) fluid mixing and drug elimination from the anterior chamber; 2) permeability of macromolecule through retina; and 3) fluid flow to the posterior direction within the vitreal cavity. These are essential features that will be useful in later scaling of the model to the human eye. This model will be a useful tool for understanding the concentration differences of injected macromolecules in the vitreous and their elimination pathways. Obviously, the model is applicable also in the pharmacokinetic simulations of controlled drug release systems that are inserted into the vitreous cavity or anterior chamber. It is important to note that the current model is suitable for the simulations of the macromolecule kinetics, but not for small molecular drugs. In order to simulate small molecular drugs, the model must be extended to include their permeability in the ocular barriers, such as blood retina barrier and blood aqueous humor barrier.

Percentage of Anterior Elimination Pathway from the Aqueous AUC

When a macromolecule is not taken up by the iris and it is eliminated from the anterior chamber solely by aqueous drainage, the amount of macromolecule eliminated via the anterior pathway after IVT injection can be estimated by multiplying the aqueous AUC (AUC_a) with aqueous humor flow rate (f) (Eq. 8). We used this equation to verify the correct mass balance in our CFD model. Furthermore, as a preliminary test of its applicability in the actual PK data analysis, we calculated from recently published *in vivo* data for four antibodies (50–150 kDa) (3) that the percentage of anterior pathway was 74–97% when using f of 2.5 µl min^{-1}, and 89–114% when using f of 3.0 µl min^{-1}, respectively (Table SVI in Electronic Supplementary Material; measured f was not

available). These values are close to those obtained with a semi-mechanistic 3-compartment model (82–87%) (3), and support the general conclusions about the dominant role of the anterior pathway in the elimination of macromolecules. The proposed calculation method places high demands for the experimental procedure including an exact dosing, an excellent injection technique, a well-designed aqueous sampling schedule, and an accurate and precise assay method. In addition, a good estimate of f is required, and the best option is to measure f in the experimental animals with topical fluorescein and *in vivo* fluorophotometry and take the diurnal variation in f into account (48,53).

Conclusions

The anatomically accurate CFD model of the rabbit eye by Missel (11) was extended for intravitreal and intracameral injections of macromolecules. The mixing in the anterior chamber was enhanced with thermal gradient, heat transfer and gravity, and this feature is expected to be essential in intracameral and topical drug administration. For intravitreal injections of FITC-dextrans the diffusion though retina was defined based on our previously published *in vitro* data, and a good match with *in vivo* data and a quantitative estimate of the percentages of the anterior and posterior elimination pathways were obtained. The extended model is a valuable tool for data interpretation and predictions.

REFERENCES

1. Wong WL, Su X, Li X, Cheung CM, Klein R, Cheng CY, et al. Global prevalence of age-related macular degeneration and disease burden projection for 2020 and 2040: a systematic review and meta-analysis. Lancet Glob Health. 2014;2(2):106–16.
2. Holz FG, Tadayoni R, Beatty S, Berger A, Cereda MG, Cortez R, et al. Multi-country real-life experience of anti-vascular endothelial growth factor therapy for wet age-related macular degeneration. Br J Ophthalmol. 2015;99(2):220–6.
3. Hutton-Smith LA, Gaffney EA, Byrne HM, Maini PK, Gadkar K, Mazer NA. Ocular pharmacokinetics of therapeutic antibodies given by intravitreal injection: estimation of retinal permeabilities using a 3-compartment semi-mechanistic model. Mol Pharm. 2017;14(8):2690–6.
4. Del Amo EM, Rimpelä AK, Heikkinen E, Kari OK, Ramsay E, Lajunen T, et al. Pharmacokinetic aspects of retinal drug delivery. Prog Retin Eye Res. 2017;57:134–85.
5. Cunha-Vaz JG, Maurice DM. The active transport of fluorescein by the retinal vessels and the retina. J Physiol. 1967;191(3):467–86.
6. Araie M, Maurice DM. The loss of fluorescein, fluorescein glucuronide and fluorescein isothiocyanate dextran from the vitreous by the anterior and retinal pathways. Exp Eye Res. 1991;52(1):27–39.
7. Tan LE, Orilla W, Hughes PM, Tsai S, Burke JA, Wilson CG. Effects of vitreous liquefaction on the intravitreal distribution of sodium fluorescein, fluorescein dextran, and fluorescent microparticles. Invest Ophthalmol Vis Sci. 2011;52(2):1111–8.
8. Kim H, Lizak MJ, Tansey G, Csaky KG, Robinson MR, Yuan P, et al. Study of ocular transport of drugs released from an intravitreal implant using magnetic resonance imaging. Ann Biomed Eng. 2005;33(2):150–64.
9. Tojo KJ, Ohtori A. Pharmacokinetic model of intravitreal drug injection. Math Biosci. 1994;123(1):59–75.
10. Friedrich S, Cheng YL, Saville B. Finite element modeling of drug distribution in the vitreous humor of the rabbit eye. Ann Biomed Eng. 1997;25(2):303–14.
11. Missel PJ. Simulating intravitreal injections in anatomically accurate models for rabbit, monkey, and human eyes. Pharm Res. 2012;29(12):3251–72.
12. Friedrich S, Cheng YL, Saville B. Drug distribution in the vitreous humor of the human eye: the effects of intravitreal injection position and volume. Curr Eye Res. 1997;16(7):663–9.
13. Tojo K, Nakagawa K, Morita Y, Ohtori A. A pharmacokinetic model of intravitreal delivery of ganciclovir. Eur J Pharm Biopharm. 1999;47(2):99–104.
14. Stay MS, Xu J, Randolph TW, Barocas VH. Computer simulation of convective and diffusive transport of controlled-release drugs in the vitreous humor. Pharm Res. 2003;20(1):96–102.
15. Balachandran RK, Barocas VH. Computer modeling of drug delivery to the posterior eye: effect of active transport and loss to choroidal blood flow. Pharm Res. 2008;25(11):2685–96.
16. Kotha S, Murtomäki L. Virtual pharmacokinetic model of human eye. Math Biosci. 2014;253:11–8.
17. Friedrich S, Saville B, Cheng YL. Drug distribution in the vitreous humor of the human eye: the effects of aphakia and changes in retinal permeability and vitreous diffusivity. J Ocul Pharmacol Ther. 1997;13(5):445–59.
18. Kathawate J, Acharya S. Computational modeling of intravitreal drug delivery in the vitreous chamber with different vitreous substitutes. Int J Heat Mass Transf. 2008;51(23):5598–609.
19. Balachandran RK, Barocas VH. Contribution of saccadic motion to intravitreal drug transport: theoretical analysis. Pharm Res. 2011;28(5):1049–64.
20. Missel PJ, Horner M, Muralikrishnan R. Simulating dissolution of intravitreal triamcinolone acetonide suspensions in an anatomically accurate rabbit eye model. Pharm Res. 2010;27(8):1530–46.
21. Tojo K. A pharmacokinetic model for ocular drug delivery. Chem Pharm Bull. 2004;52(11):1290–4.
22. Ueda K, Ohtori A, Tojo K. Effects of pathological conditions on ocular pharmacokinetics of antimicrobial drugs. Chem Pharm Bull. 2010;58(10):1301–5.
23. Shikamura Y, Ohtori A, Tojo K. Drug penetration of the posterior eye tissues after topical instillation: in vivo and in silico simulation. Chem Pharm Bull. 2011;59(10):1263–7.
24. Park J, Bungay PM, Lutz RJ, Augsburger JJ, Millard RW, Sinha Roy A, et al. Evaluation of coupled convective-diffusive transport of drugs administered by intravitreal injection and controlled release implant. J Control Release. 2005;105(3):279–95.

25. Krishnamoorthy MK, Park J, Augsburger JJ, Banerjee RK. Effect of retinal permeability, diffusivity, and aqueous humor hydrodynamics on pharmacokinetics of drugs in the eye. J Ocul Pharmacol Ther. 2008;24(3):255–67.

26. Wyatt HJ. Ocular pharmacokinetics and convectional flow: evidence from spatio-temporal analysis of mydriasis. J Ocul Pharmacol Ther. 1996;12(4):441–59.

27. Wyatt HJ. Modelling transport in the anterior segment of the eye. Optom Vis Sci. 2004;81(4):272–82.

28. Canning CR, Greaney MJ, Dewynne JN, Fitt AD. Fluid flow in the anterior chamber of a human eye. IMA J Math Appl Med Biol. 2002;19(1):31–60.

29. Heys JJ, Barocas VH. A boussinesq model of natural convection in the human eye and the formation of Krukenberg's spindle. Ann Biomed Eng. 2002;30(3):392–401.

30. Johnson F, Maurice D. A simple method of measuring aqueous humor flow with intravitreal fluoresceinated dextrans. Exp Eye Res. 1984;39(6):791–805.

31. Araie M. Time change of rabbit aqueous flow under influence of adrenergic drugs. Exp Eye Res. 1985;41(3):391–403.

32. Pitkänen L, Ranta V, Moilanen H, Urtti A. Permeability of retinal pigment epithelium: effects of permeant molecular weight and lipophilicity. Invest Ophthalmol Vis Sci. 2005;46(2):641–6.

33. Cantrill HL, Pederson JE. Experimental retinal detachment. VI. The permeability of the blood-retinal barrier. Arch Ophthalmol. 1984;102(5):747–51.

34. Hirata A, Watanabe S, Kojima M, Hata I, Wake K, Taki M, et al. Computational verification of anesthesia effect on temperature variations in rabbit eyes exposed to 2.45 GHz microwave energy. Bioelectromagnetics. 2006;27(8):602–12.

35. Ng EYK, Ooi EH. FEM simulation of the eye structure with bio-heat analysis. Comput Methods Prog Biomed. 2006;82(3):268–76.

36. Lagendijk JJ. A mathematical model to calculate temperature distributions in human and rabbit eyes during hyperthermic treatment. Phys Med Biol. 1982;27(11):1301–11.

37. Bill A. Blood circulation and fluid dynamics in the eye. Physiol Rev. 1975;55(3):383–417.

38. Karampatzakis A, Samaras T. Numerical model of heat transfer in the human eye with consideration of fluid dynamics of the aqueous humour. Phys Med Biol. 2010;55(19):5653–65.

39. Schwartz B, Feller MR. Temperature gradients in the rabbit eye. Investig Ophthalmol. 1962;1:513–21.

40. Lorget F, Parenteau A, Carrier M, Lambert D, Gueorguieva A, Schuetz C, et al. Characterization of the pH and temperature in the rabbit, pig, and monkey eye: key parameters for the development of long-acting delivery ocular strategies. Mol Pharm. 2016;13(9): 2891–6.

41. Laurent TC, Ryan M, Pietruszkiewicz A. Fractionation of hyaluronic acid. The polydispersity of hyaluronic acid from the bovine vitreous body. Biochim Biophys Acta. 1960;42:476–85.

42. Amirpour N, Karamali F, Razavi S, Esfandiari E, Nasr-Esfahani MH. A proper protocol for isolation of retinal pigment epithelium from rabbit eyes. Adv Biomed Res. 2014;3:4.

43. Zhou J, He S, Zhang N, Spee C, Zhou P, Ryan SJ, et al. Neutrophils compromise retinal pigment epithelial barrier integrity. J Biomed Biotechnol. 2010;2010:289360.

44. Braeckmans K, Peeters L, Sanders NN, De Smedt SC, Demeester J. Three-dimensional fluorescence recovery after photobleaching with the confocal scanning laser microscope. Biophys J. 2003;85(4):2240–52.

45. Laurent UB, Fraser JR. Turnover of hyaluronate in the aqueous humour and vitreous body of the rabbit. Exp Eye Res. 1983;36(4): 493–503.

46. Maurice DM. Injection of drugs into the vitreous body. In: Leopold I, Burns R, editors. Symposium on ocular therapy, vol. 9. London: Wiley; 1976. p. 59–72.

47. Maurice DM, Mishima S. Ocular pharmacology. In: Sears M, editor. Handbook of experimental pharmacology. Berlin-Heidelberg: Springer-Verlag; 1984. p. 16–119.

48. Yablonski ME, Hayashi M, Cook DJ, Chubak G, Sirota M. Fluorophotometric study of intravenous carbonic anhydrase inhibitors in rabbits. Invest Ophthalmol Vis Sci. 1987;28(12):2076–82.

49. Hutton-Smith LA, Gaffney EA, Byrne HM, Maini PK, Schwab D, Mazer NA. A mechanistic model of the intravitreal pharmacokinetics of large molecules and the pharmacodynamic suppression of ocular vascular endothelial growth factor levels by ranibizumab in patients with neovascular age-related macular degeneration. Mol Pharm. 2016;13(9):2941–50.

50. Schmitt W. Estimation of intra-vitreal half-lifes in the rabbit eye with semi-mechanistic equations. Pharm Res. 2017;34(1):49–57.

51. Maurice DM. Protein dynamics in the eye studied with labelled proteins. Am J Ophthalmol. 1959;47(1 Pt 2):361–8.

52. Haghjou N, Abdekhodaie MJ, Cheng Y. Retina-choroid-sclera permeability for ophthalmic drugs in the vitreous to blood direction: quantitative assessment. Pharm Res. 2013;30(1):41–59.

53. Zhao M, Hejkal JJ, Camras CB, Toris CB. Aqueous humor dynamics during the day and night in juvenile and adult rabbits. Invest Ophthalmol Vis Sci. 2010;51(6):3145–51.